Search for the Fermi-surface anomaly in fast-neutron scattering from yttrium

R. D. Lawson, P. T. Guenther, and A. B. Smith
Applied Physics Division, Argonne National Laboratory, Argonne, Illinois 60439
(Received 25 June 1986)

Neutron differential-elastic-scattering cross sections of yttrium were measured from 4 to 10 MeV, at energy intervals of approximately 500 keV, and at 20 or more angles distributed between 20° and 160°. The results were combined with data previously reported from this laboratory to obtain a detailed data base extending from 1.5 to 10.0 MeV. These data were interpreted using a spherical optical-statistical model, including the surface-peaked real potential predicted by the use of dispersion relations. The volume integral of the real potential, J_V, was found to decrease linearly with energy, and that energy dependence was accounted for using the dispersion relationship linking the real and imaginary potentials. Thus, in the energy range of the present measurements, the neutron interaction with ^{89}Y does not display a Fermi-surface anomaly of the nature reported in the ^{208}Pb region. On the other hand, the energy dependence of J_V needed to give the correct binding energies for the single-particle and single-hole states did tend toward constant values with decreasing energy, as expected, and perhaps even a decrease is suggested by some of the hole states.

I. INTRODUCTION

It was pointed out many years ago[1] that near the Fermi surface the effective mass, m^*, of a valence nucleon is nearly equal to its free mass, m. Evidence of this is provided by, for example, the observed single-particle and single-hole energy spacings near ^{208}Pb, which agree quite well with those predicted from a static Woods-Saxon potential.[2] The ratio m^*/m is related to the rate of change of the real potential with energy[3] by

$$m^*/m = 1 - \frac{dV}{dE} , \tag{1}$$

so that $m^*/m \approx 1$ implies $dV/dE \approx 0$ near the Fermi surface. Recently, Mahaux and Ngô[4] have made a detailed study of the polarization and correlation contributions to the optical-model potential for the doubly-closed-shell nuclei ^{40}Ca and ^{208}Pb. They suggest that in these nuclei, below about 6.0 MeV, the real potential has a highly nonlinear energy dependence. Experimental neutron scattering in the ^{208}Pb region supports these theoretical predictions.[5,6] However, an optical-model interpretation of low-energy neutron scattering from doubly magic nuclei is very difficult due to cross-section fluctuations. In view of this it is productive to search for the above anomaly in a mass region where fluctuations are less of a hindrance, and where an energy-averaged cross section consistent with the concept of the optical model can be determined to much lower energies. Such an investigation was recently carried out using the essentially spherical target ^{93}Nb.[7] The results of the latter study did not reveal an anomalous behavior of the optical-model potential of the nature predicted, and experimentally observed, for ^{208}Pb. In this paper we present the results of a similar study of neutron scattering from another spherical nucleus in this mass region, ^{89}Y. The data base consists of neutron differential-elastic-scattering cross sections over the energy range 1.5–10.0 MeV. These data were analyzed using two variants of the optical-statistical model. First, a conventional calculation was made in which the real potential had the Woods-Saxon form, the imaginary potential a derivative Woods-Saxon well, and the spin-orbit interaction was represented by a potential of the Thomas form. A second analysis was made in which the real surface-peaked interaction, predicted by the use of dispersion relations,[3] was added to the above potential. The results of both analyses led to a volume integral of the real potential, J_V, that decreased linearly with increasing energy over the entire energy range of the present measurements. On the other hand, if one examines the values of J_V needed to obtain the correct binding energies for the single-particle and single-hole states in this nucleus, one sees a flattening out of J_V ($dV/dE \approx 0$), and perhaps even a decrease, with decreasing energy. Thus at negative energies the expected deviation from linearity is indeed evident. However, as previously found in ^{93}Nb, neutron scattering in the energy range 1.5–10 MeV shows little, if any, evidence for the Fermi-surface anomaly in ^{89}Y of the nature and magnitude reported in the ^{208}Pb region.

II. EXPERIMENTAL METHODS AND RESULTS

All of the measurements were made using the Argonne multiangle time-of-flight system.[8] That apparatus, and its application to measurements of the present type, has been extensively described by Budtz-Jørgensen *et al.*[9] and Smith *et al.*,[10] and thus is not further discussed in detail here. The scattering sample was a solid yttrium cylinder, 2 cm in diameter and 2 cm long. Scattered-neutron velocity resolutions were sufficient to resolve the elastically scattered neutrons from known inelastically scattered ones at all the measured incident energies. Below 4.0 MeV the scattering cross sections were determined relative to the neutron total cross sections of elemental carbon, as recently reported by Budtz-Jørgensen *et al.*[9] The present measurements, above 4.0 MeV, were determined relative to the

well-known H(n,n)H cross sections.[11] The relative angles were determined to approximately $\pm 0.1°$, and the absolute ones to better than $\pm 0.5°$. All of the yttrium and reference-standard measurements were corrected for multiple-event, beam-attenuation, and angular-resolution perturbations using the methods described by Guenther.[12] At the higher incident energies, the multiple-event corrections required several iterations from the observed values for acceptable convergence.

The present elastic-scattering measurements extended from 4.5 to 10.0 MeV, in steps of approximately 500 keV. The incident-neutron energy spreads were approximately 300 keV at 4.5 MeV, and decreased to about 100 keV at 10.0 MeV. Measurements were made at a minimum of 20 scattering angles at each incident energy, distributed between 20° and 160°. At most energies there were 35—40 measurements, and more at some energies. The measurements were distributed over a several-year period, with essentially independent experimental arrangements. The results obtained at these different times were in good agreement. The fidelity of the measurement system was verified at each energy by concurrent measurements of the well-known differential-elastic-scattering cross sections of carbon.[11]

The present data were combined with the lower-energy (i.e., below 4.0 MeV) values recently reported from this laboratory[9] to obtain the comprehensive data set shown in Fig. 1. In the present measurements the systematic normalization uncertainties were approximately 3%. Statistical errors were very small (less than 1%) in regions of relatively large cross sections, and increased to larger values in the minima of the distributions. Correction procedures introduced an additional factor of approximately 1%, with again larger values in the minima of the distributions. The uncertainty associated with the above-cited angular deviations was relatively large at some angles. These various components were combined in quadrature to obtain the total error. There are very few previous experimental results comparable with the present data, and most of them are very old and of lesser quality. Exceptions are the works of Kinney and Perey[13] and Walter *et al.*[14] The results of Ref. 13 are reasonably consistent with those of the present work, though they do not have the angular coverage of the present data. Comparisons with the results of Ref. 14 are limited to the 8.0 and 10.0 MeV distributions. Within this limited scope and from the available graphical information, the results of Ref. 14 seem to agree with those of the present work.

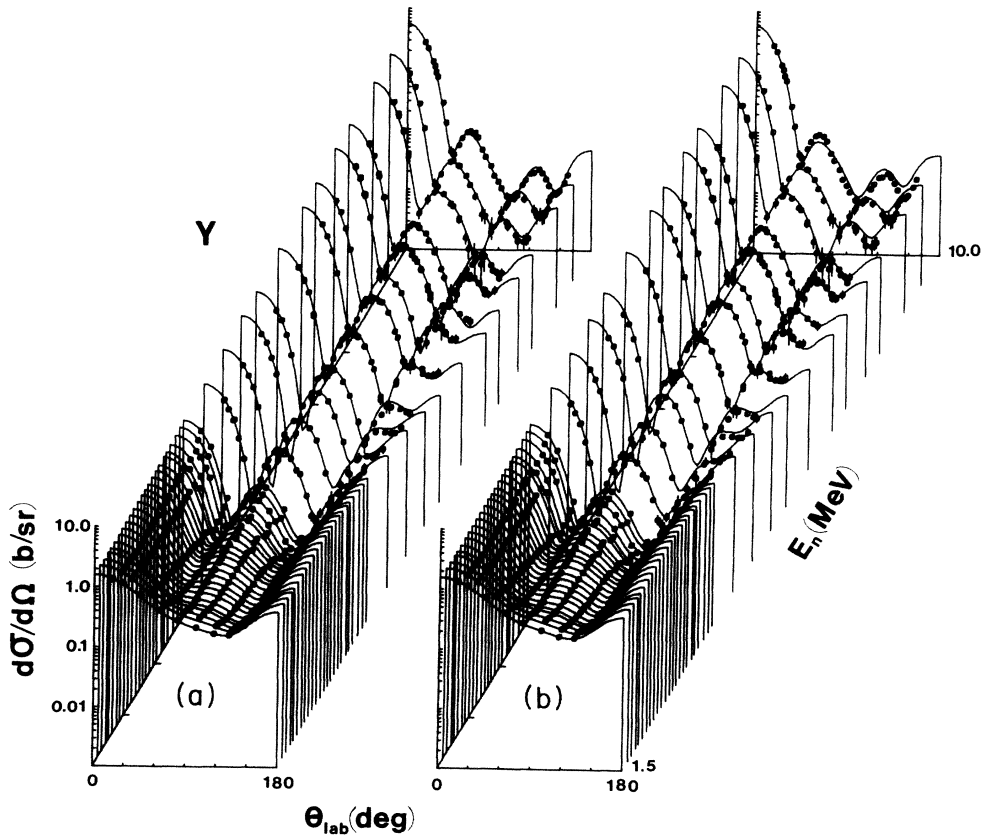

FIG. 1. Comparison of measured and calculated neutron differential-elastic-scattering cross sections of ^{89}Y. The measured values are indicated by data symbols. Curves in (a) show the result when a three parameter fit, in which a_v, V, and W were varied, was made to the data. In this fit r_v, the imaginary geometry, and the spin-orbit potential were given by Eqs. (3), (4), and (5), respectively. Curve (b) is the result obtained when the optical model potential was parametrized by Eqs. (3)—(5) and (9)—(11).

The above data base was felt to be of sufficient angle and energy scope and experimental accuracy for quantitative assessment of the optical-potential energy dependence and its implications with respect to the Fermi-surface anomaly.

III. INTERPRETATION AND METHODS

Our analysis of the experimental data was carried out assuming that, in the energy range of interest, the neutron total and elastic-scattering cross sections of yttrium can be described in terms of a spherical optical-statistical model.[15] However, the analysis differs from the one we recently reported[7] for another nucleus in this mass region, ^{93}Nb, in three respects.

A. Error interpretation

In fitting the optical-model parameters to "N" experimental data, one minimizes the function

$$\chi^2=\sum_{i=1}^{N}\left[\frac{\sigma_{\text{expt}}(i)-\sigma_{\text{theory}}(i)}{\delta\sigma_{\text{expt}}(i)}\right]^2, \tag{2}$$

where $\delta\sigma_{\text{expt}}(i)$ is the uncertainty in the ith measurement. In the case of ^{93}Nb, $\delta\sigma_{\text{expt}}(i)$ was assumed to be statistical and thus, for our experimental method, is approximately proportional to the square root of the cross section at angle $\theta(i)$. In the present yttrium analysis we have refined our estimates by taking into account not only the statistical error but also the other elements of the experimental uncertainties outlined above. $\delta\sigma_{\text{expt}}(i)$ of Eq. (2) is taken to be the rms value of these error components. In regions where the cross section is rapidly changing with angle, $\delta\sigma_{\text{expt}}(i)$ is dominated by the angular uncertainty.

B. Parameter energy dependence

In the present analysis, and that of the prior ^{93}Nb study, we assume that the real potential has the Woods-Saxon form, the imaginary potential the Woods-Saxon-derivative shape, and the spin-orbit potential the Thomas form.[15] In the ^{93}Nb study the spin-orbit geometry was taken equal to that of the real potential, all potential geometric factors were assumed to be energy independent, and only the real (V) and imaginary (W) well depths were allowed to vary with energy. In the present yttrium interpretation, some of these constancy conditions are relaxed.

A six-parameter fitting survey of the 1.5–10 MeV yttrium data indicated that the real-potential radius, r_v ($R_v=r_vA^{1/3}$), did not vary significantly with energy and had an average value of

$$r_v=1.24\text{ fm}. \tag{3}$$

This is essentially the same result as found in interpreting the 1.5–4.0 MeV data for a number of nuclei in this mass region.[16] Partly because of this and partly because of the strong anticorrelation between r_v and V, r_v was held fixed at this value in all subsequent calculations. On the other hand, interpretation of the ^{93}Nb data using an energy independent imaginary radius, r_w, and diffuseness, a_w, was found to be difficult, and this was also indicated by our survey.[7,17] Thus we decided to allow a linear energy dependence of these two quantities in the discussion of the yttrium data. Fits to experiment at 5.0 and 10.0 MeV, judged to be of "best" quality, lead to energy variations of

$$a_w=0.1661+0.0284E\text{ fm},$$
$$\text{and} \tag{4}$$
$$r_w=1.5336-0.0255E\text{ fm},$$

where E is the incident-neutron laboratory energy in MeV. These linear expressions were then used to obtain r_w and a_w at other energies.

Interpretation of the higher-energy and larger-angle distributions indicated a spin-orbit-potential geometry considerably different from that of the real potential. Detailed fitting of the 8.03 and 10.0 MeV distributions lead to the selection of the following spin-orbit parameters,

$$V_{\text{so}}=5.75\text{ MeV},$$
$$r_{\text{so}}=1.025\text{ fm}, \tag{5}$$
$$a_{\text{so}}=0.4\text{ fm},$$

and these values were held fixed throughout the remainder of the yttrium interpretation. They are similar to those found in polarization studies in this mass-energy region.[14]

With the above constraints, each distribution was fitted by simultaneously varying the well-depth parameters V and W and the real diffuseness, a_v. At the higher energies (above approximately 8.0 MeV) the neutron total cross section[10] was included in the fitting procedure to assure proper physical behavior at very small scattering angles (i.e., consistency with Wick's Limit).[18] All of the fitting was done using the computer code ABAREX.[19] Compound-nucleus contributions were calculated using the Hauser-Feshbach formula,[20] as modified by Moldauer.[21] Thirteen discrete excited levels were included in the calculations using the energies and spin-parity assignments given by Lederer and Shirley.[22] Excitations above 3.2 MeV were included in the calculations using the statistical formalism and parameters of Gilbert and Cameron.[23] The low-energy portion of the data base may be subject to fluctuations. Therefore, all the elastic-scattering distributions below 4.0 MeV were concurrently fitted, resulting in energy-averaged optical-model parameters at a mean energy of 2.75 MeV. Above 4.0 MeV the distributions were treated individually.

C. Inclusion of a surface real potential

In the analysis discussed above, the real optical-model potential was assumed to have a Woods-Saxon form. However, there is a dispersion relationship between the real and imaginary interactions,[3]

$$V(r,E)=V_1(r,E)+\frac{\text{P}}{\pi}\int_{-\infty}^{\infty}\frac{W(r,E')}{E-E'}dE', \tag{6}$$

where $V_1(r,E)$ is the Hartree-Fock real potential (which we assume to have the Woods-Saxon shape) and P stands for the principal-value integral. Thus, if the radial form

of the imaginary potential, $W(r,E')$, is surface peaked (as in the above interpretation), Eq. (6) predicts that the real potential should have a surface-peaked component. Therefore, we have carried out a second fitting of the yttrium data, including this surface-peaked real component, but still requiring the parameter constraints of Eqs. (3)—(5).

IV. INTERPRETATION AND RESULTS

In this section we discuss the results of the above-outlined fitting procedures for two cases: (i) simple Woods-Saxon real potential, and (ii) with the addition of the surface-peaked real component predicted by the dispersion relationship of Eq. (6).

A. Conventional Woods-Saxon real potential

With the constraints of Eqs. (3)—(5), V, a_v, and W were concurrently varied to best fit the observed neutron total and differential-elastic-scattering cross sections. Thirteen energies were involved in the fitting: 2.75 (simultaneous fitting of all results in the 1.5—4.0 MeV range), 4.5, 5.0, 5.5, 5.9, 6.5, 7.1, 7.5, 8.03, 8.4, 9.05, 9.5, and 10.0 MeV. Good descriptions of the observed differential-elastic-scattering cross sections were obtained, as shown in Fig. 1(a).

The parameters obtained from the above fitting are plotted in Fig. 2 as a function of energy. These are the real diffuseness (a_v) and the volume integrals of the real (J_V) and imaginary (J_W) potentials. For the Woods-Saxon and Woods-Saxon-derivative wells, the volume integrals are approximately given by[24]

$$J_V=\frac{4\pi}{A}\int V(r)r^2dr \approx \frac{4\pi}{3}r_v^3V_0\left[1+\left[\frac{\pi a_v}{R_v}\right]^2\right] \quad (7)$$

and

$$J_W=\frac{4\pi}{A}\int W(r)r^2dr \approx \frac{16\pi}{A}R_w^2a_wW_0\left[1+\frac{1}{3}\left[\frac{\pi a_w}{R_w}\right]^2\right], \quad (8)$$

respectively, where V_0 and W_0 are the real and imaginary well depths, and in the present case the atomic number is $A=89$.

In order to examine the energy dependences of the parameters of Fig. 2, one must assign them errors extracted from the fitting procedures. We assume that the uncertainty at energy E is proportional to the value of χ^2/N (where N is the number of observables at energy E) and χ^2 is given by Eq. (2). The proportionality constant is chosen separately for each parameter (a_v, J_V, and J_W), so that χ^2 per degree of freedom for each curve of Fig. 2 has a value of unity. Since the minimum χ^2/N occurs for the 7.5 MeV data, the errors shown in Fig. 2 are smallest at that energy. With these error assumptions, one finds that a_v and J_W are energy independent, with values of

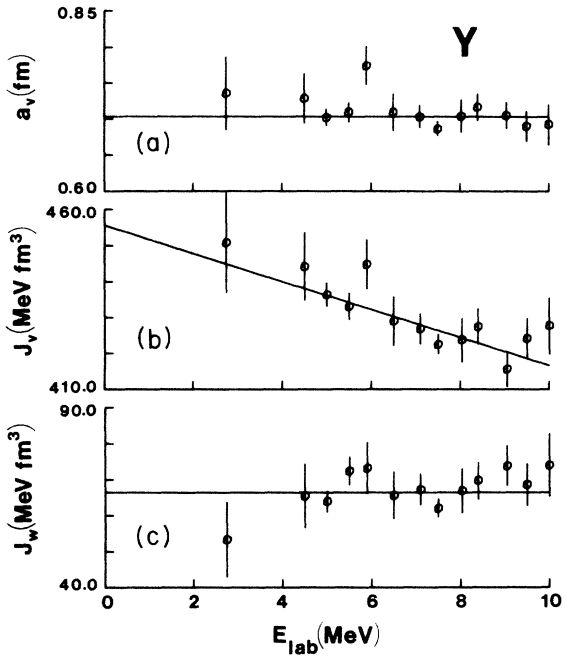

FIG. 2. The behavior, as a function of laboratory energy, of the diffuseness, a_v, of (a) the real potential and the volume integrals of (b) the real, J_V, and (c) imaginary, J_W, potentials. The line in each case is the best fit to the data [Eqs. (9)—(11) of the text]. The error bars are assigned as discussed in the text and their normalizations are chosen to give a χ^2 per degree of freedom for each fit of unity.

$$a_v=0.7033\pm0.0049 \text{ fm} \quad (9)$$

and

$$J_W=66.47\pm1.29 \text{ MeV fm}^3 . \quad (10)$$

However, J_V shows a significant energy variation given by

$$J_V=(455.64\pm5.96)-(3.89\pm0.83)E \text{ MeV fm}^3 , \quad (11)$$

with the errors in the coefficients almost exactly anticorrelated. The uncertainties given in Eqs. (9)—(11) depend on the fact that we have assumed χ^2 per degree of freedom is unity in each case. This corresponds to an error in a_v, J_V, and J_W at 7.5 MeV of 1.46%, 0.63%, and 4.01%, respectively. Thus, of the three quantities, J_W is the least well determined.

From an inspection of Fig. 2, it is evident that the 5.9 MeV data leads to a_v and J_V parameters that are considerably larger than those at neighboring energies. If one were to neglect the 5.9 MeV data, and there is no *a priori* reason to do so, the above conclusions as to parameter energy dependences would not significantly change. Equations (9)—(11) would become only slightly different:

$$a_v=0.7009\pm0.0033 \text{ fm} ,$$

$$J_W=66.23\pm1.31 \text{ MeV fm}^3 ,$$

and

$$J_V=(453.69\pm5.23)-(3.68\pm0.73)E \text{ MeV fm}^3 .$$

These changes are within the respective quoted uncertainties.

In Fig. 1(b) the results obtained when the optical model potential is parametrized by Eqs. (3)—(5) and (9)—(11) are compared with experiment. From inspection of Figs. 1(a) and 1(b) one sees that up to about 8 MeV this characterization reproduces experiment as well as does the explicit three-parameter fit. On the other hand, above 8 MeV the explicit fit represents the data somewhat better. This may be due to a slight flattening out of J_V at the higher energies—a conclusion which is not at variance with the results shown in Fig. 2(b). This possible behavior will be further discussed later.

B. Results with a surfaced-peaked real potential

If the imaginary potential $W(r,E')$ is surface peaked, Eq. (6) predicts that there should be a surface component to the real potential. In order to estimate its strength one must know $W(r,E')$ for all energies, E', while our experiments only give information from 1.5 to 10 MeV. A further complication is the energy-dependent geometry of W. To simplify matters we have estimated the strength of the surface real potential using the volume integral of the imaginary potential in the following way:

(i) In the range $0 \leq E' \leq 13.77$ MeV we assume $J_W(E')$ is given by Eq. (10).

(ii) For $13.77 \leq E' \leq 57.22$ MeV we calculate, from the potential of Walter and Guss,[14]

$$J_W(E') = 87.54 - 1.53E' \text{ MeV fm}^3 . \quad (10')$$

At 13.77 MeV, Eqs. (10) and (10') give the same values of J_W so the function is continuous. Furthermore, the Walter-Guss potential implies that J_W vanishes at 57.22 MeV.

(iii) On the basis of the dilute Fermi-gas model, it can be shown[25] that near the Fermi energy (approximately -9.1 MeV for ^{89}Y) $W(E')$ is proportional to $(E'-E_F)^2$. Thus for $-18.2 \leq E' \leq 0$ MeV we assume

$$J_W(E') = 0.8029(E'+9.1)^2 \text{ MeV fm}^3 . \quad (10'')$$

With these assumptions, $J_W(E')$ has a continuous value over the range $-18.2 \leq E' \leq 57.22$ MeV. When Eqs. (10), (10'), and (10'') are inserted into the dispersion relationship, one calculates the volume integral of the surface-peaked part of the real potential from

$$J_R(E) = \frac{\mathrm{P}}{\pi} \int_{-18.2}^{57.22} \frac{J_W(E')dE'}{E-E'} . \quad (12)$$

The result is indicated by the curve in Fig. 3(a).

Clearly, $J_R(E)$ is sensitive to what one assumes for $J_W(E')$ when $E' \leq 0$. An alternative assumption was made by Annand, Finlay, and Dietrich,[6] namely that $J_W(E')=0$ when $E' \leq 0$. Under these conditions, $J_R(E)$ is predicted to be larger than shown in Fig. 3(a). Using Eqs. (10) and (10') in Eq. (12), one changes the predicted value of $J_R(E)$ at $E=2.75$ MeV from 32.85 to 50.60 MeV fm^3, and at 10.0 MeV from 8.51 to 16.32 MeV fm^3. However,

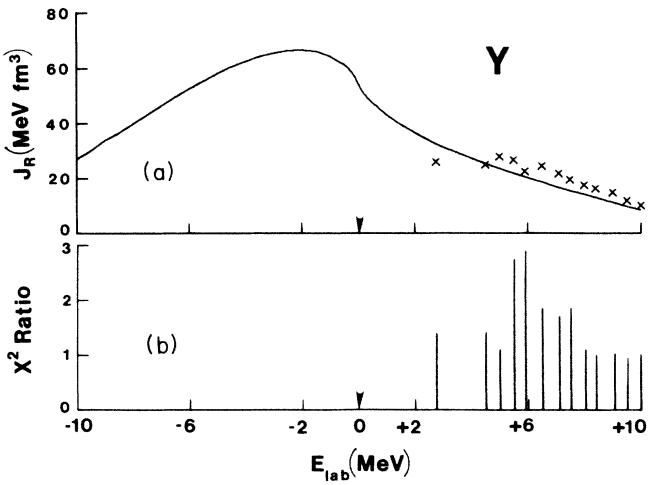

FIG. 3. (a) The integral $J_R(E)$ [from Eqs. (10) and (12) of the text] is plotted as a function of energy. The $\times$ symbols are the values after one iteration [i.e., the volume integral of Eq. (14a) is evaluated using the new value of W]. (b) The ratio of χ^2 obtained when ΔV of Eqs. (14) is included compared to the value with $\Delta V=0$ (i.e., the conventional optical model).

under these conditions $J_R(E)$ has a logarithmic singularity as $E \to 0$. One can get around this difficulty by parametrizing $J_W(E')$ in a manner similar to that proposed by Ahmad and Haider.[26] A reasonable fit to the $J_W(E')$ values given by Eqs. (10) and (10') is obtained if one assumes

$$J_W(E') = (18.74E')\exp(-0.092\,524E') \text{ MeV fm}^3 . \quad (13)$$

When this is used in Eq. (12), the predicted $J_R(E)$ values are even larger: 71.08 MeV fm^3 at 2.75 MeV and 24.47 MeV fm^3 at 10.0 MeV. Setting $J_W(E')=0$ at $E'=0$ is not physically attractive. The low-energy scattering data show no evidence for volume absorption and, if the surface absorption vanishes at $E'=0$, the S-wave strength function also vanishes, in contradiction to experiment.

The above values of $J_R(E)$, predicted using Eqs. (10) and (12), are probably uncertain by something like a factor of 2. However, as we shall see, the final results are not too sensitive to moderate changes in $J_R(E)$, and so throughout the remainder of this discussion we shall use the values computed with Eqs. (10). We add to the real Woods-Saxon potential a real derivative Woods-Saxon well given by

$$\Delta V = 4\lambda(E) W_0 a_w \frac{d}{dr}\left\{\frac{1}{1+\exp[(r-r_w A^{1/3})/a_w]}\right\} , \quad (14a)$$

where

$$\lambda(E) = J_R(E)/J_W(E) . \quad (14b)$$

With this added potential, and the constraints of Eqs. (3)—(5), a best fit to the data was made by again varying V, a_v, and W. Since W was allowed to vary, the fitting

should have been done in an iterative manner, i.e., after a fit, the values of $J_R(E)$ should be recalculated, a new value of ΔV computed, and then the fit repeated. In Fig. 3(a), the $\times$ symbols indicate the volume integral of J_R after one iteration. These values do not show a $J_R(E)$ greatly different from that calculated from Eqs. (10). Thus, in view of the uncertainties in the calculation of $J_R(E)$, only one iteration was carried out.

The fit to the experimental data using the surface-peaked real potential was generally not as good as that obtained using the conventional optical model discussed in the preceding subsection. In Fig. 3(b) we plot the ratio of χ^2, Eq. (2), obtained when the ΔV term is included, to that without it. Except at 5 MeV, the conventional optical model results in a significantly better fit below 8.0 MeV. Above 8.0 MeV, where ΔV is small, the fits are comparable, and in fact at 9.5 MeV the fit with ΔV included is somewhat better.

In deducing the energy dependence of the model parameters, we have once again assumed that the uncertainty is proportional to the value of χ^2/N at the respective energy. The proportionality constants were chosen so that χ^2 per degree of freedom for the quadratic fit of Fig. 4(a) and the linear curves shown in Figs. 4(b) and 5 were unity. Since the minimum of χ^2/N was obtained at 5.0 MeV, the uncertainties shown in these figures are smallest at that energy. Figure 4 illustrates the values obtained for the real Woods-Saxon well parameters. In the previous fit, the diffuseness, a_v, was independent of energy, whereas now we find that a_v varies quadratically with incident energy [see curve with "tick" marks in Fig. 4(a)] as

$$a_v = \alpha + \beta E + \gamma E^2 , \tag{15a}$$

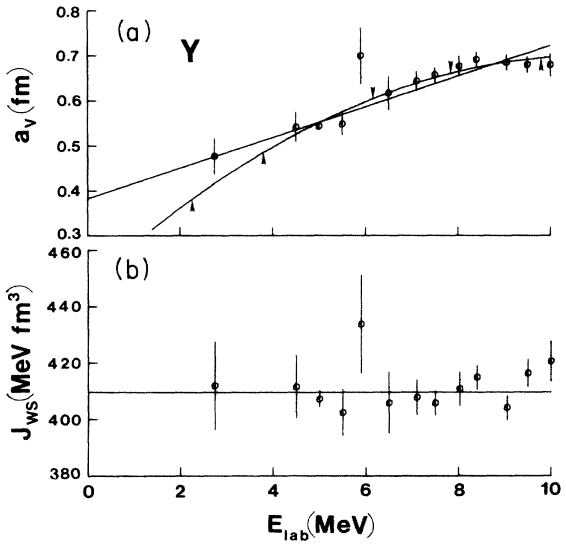

FIG. 4. The diffuseness (a_v) and volume integral (J_{WS}) of the real Woods-Saxon potential as a function of laboratory energy. Both a linear and quadratic (curve with "tick" marks) fit to the a_v data are shown. The error bars are assigned as discussed in the text and their magnitudes chosen to give a χ^2 per degree of freedom of unity for the quadratic fit to a_v and the constant value for J_{WS}.

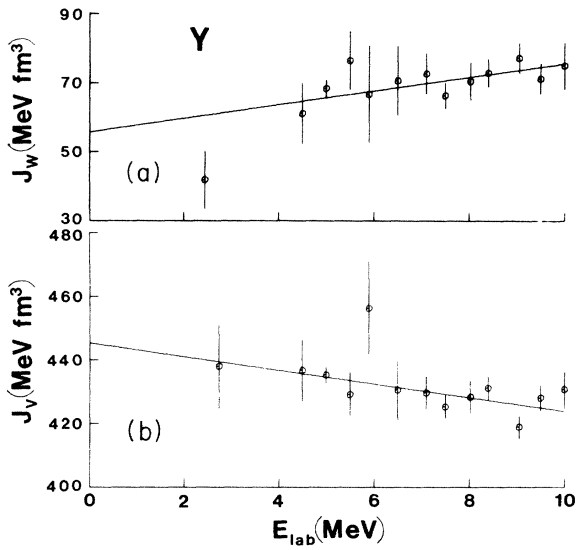

FIG. 5. The behavior, as a function of laboratory energy, of the volume integral of (a) the imaginary, J_W, and (b) the total real, J_V, potentials, including the surface-peaked contribution. The analytical expressions for the fits to the data indicated by the lines are given by Eqs. (17) and (19) of the text.

where

$$\alpha = 0.1916 \pm 0.0815 \text{ fm} ,$$
$$\beta = 0.0936 \pm 0.0248 \text{ fm/MeV} , \tag{15b}$$
$$\gamma = -(0.0043 \pm 0.0018) \text{ fm/MeV}^2 .$$

The errors in the coefficients of Eq. (15b) are based upon the assumption that the uncertainty in the 5.0 MeV value of a_v is 1.57% (quite comparable to the 1.46% value obtained in the conventional fit). The uncertainties in (α,β) and (β,γ) are almost exactly anticorrelated, while those in (α,γ) are directly correlated. Also shown in Fig. 4(a) is the result one would obtain with a linear fit to a_v [$a_v = (0.3831 \pm 0.0193) + (0.0339 \pm 0.0027)E$ fm]. However, in this case χ^2 per degree of freedom is 1.44, which is significantly larger than for the quadratic fit. Thus it seems clear that, when the contribution of Eqs. (14) is included, a_v has a quadratic energy dependence.

The fact that a_v now exhibits an energy dependence can be easily understood. The addition of ΔV, Eq. (14a), to the real volume potential is a surface effect which tends to increase the radial extent of the real well (i.e., leads to an effective a_v which is larger than that of the Woods-Saxon well alone). On the other hand, a generally better fit to the data is obtained when the conventional optical model is used. Thus, to compensate for the ΔV term, the Woods-Saxon well in the fits of this section must have a smaller a_v than previously obtained. Since ΔV is largest at lower energies, the changes will be most at such energies. Moreover, since ΔV becomes small as $E \rightarrow 10.0$ MeV, the change in $a_v \rightarrow 0$ at this energy, which is exactly the behavior given by Eqs. (15).

The volume integral, J_{WS}, of the Woods-Saxon portion

of the well is shown in Fig. 4(b). When the error in the 5.0 MeV value is taken to be 0.7%, the best fit to the data is an energy-independent parametrization with

$$J_{WS}=409.56\pm1.51 \text{ MeV fm}^3 . \quad (16)$$

We also looked at the possibility of a linear energy dependence of J_{WS}, but when this was included the χ^2 per degree of freedom only decreased from unity to 0.91 and there was a large uncertainty in the linear coefficient,

$$J_{WS}=(401.16\pm6.18)+(1.16\pm0.83)E \text{ MeV fm}^3 .$$

Thus the data give no evidence for an energy dependence of J_{WS}. This result is consistent with our previous analysis of the ^{93}Nb data,[7] where we found that the entire energy dependence of the volume integral of the real potential came from the principal-value integral of Eq. (6).

Except for the 2.75 MeV value, the volume integrals of the imaginary potential, shown in Fig. 5(a), tend to be about 4.5% larger than those found in the conventional optical-model fit. This, coupled with the fact that J_W for the 2.75 MeV energy is lower, leads to a linear increase in J_W with energy given by

$$J_W=(55.73\pm5.25)+(2.00\pm0.72)E \text{ MeV fm}^3 , \quad (17)$$

where the anticorrelated uncertainties are based on a 3.71% error for the 5.0 MeV data value. An energy independent fit to the J_W values leads to a significantly worse χ^2 per degree of freedom, 1.56, with $J_W=69.87\pm1.36$ MeV fm^3.

For this fit, the total volume integral of the real potential is the sum of two terms,

$$J_V=J_{WS}+\lambda(E)J_W , \quad (18)$$

where J_{WS}, shown in Fig. 4(b), is given by Eq. (16). J_W is characterized by Eq. (17) and shown in Fig. 5(a), and $\lambda(E)$, given by Eq. (14b), is computed using the imaginary potential described by Eqs. (10). The value of J_V obtained in this way shows a linear decrease with increasing energy [see Fig. 5(b)], described by

$$J_V=(445.30\pm5.32)-(2.14\pm0.71)E \text{ MeV fm}^3 . \quad (19)$$

Comparing Eqs. (16) and (19), it is clear that $\lambda(E)J_W$ contributes $\approx10\%$ to J_V. Thus small changes in $\lambda(E)$ [e.g., brought about by carrying out the calculation in a self-consistent manner and/or by using a different parametrization than given by Eqs. (10)], would result in only small changes in J_V.

From Figs. 4 and 5 it is clear that the 5.9 MeV data lie well off the best-fit curves describing all the other data. However, even if we were to delete this energy from the interpretation, none of the conclusions pertaining to the energy dependencies of the parameters resulting from the fit would significantly change.

V. DISCUSSION AND CONCLUSIONS

As we have seen, the conventional optical-statistical model fit to neutron total and elastic-scattering cross sections of ^{89}Y over the energy region 1.5–10.0 MeV leads to a real Woods-Saxon potential with energy-independent geometry and an energy-dependent strength given by $V=49.21-0.42E$ MeV. This energy dependence is somewhat stronger than the $-0.31E$ MeV of Rapaport's global potential,[24] and the $-0.25E$ MeV found from an analysis of similar ^{93}Nb data.[7] This is not surprising in view of the respective parameter uncertainties and the slight variations to be expected in optical-model parameters from nucleus to nucleus. Moreover, for analyses that explicitly apply to ^{89}Y, the volume integral of our potential agrees quite well with other determinations. For example, studies of 7.75 MeV neutron differential-elastic-scattering cross sections and polarization data by the Stuttgart group[27] resulted in $J_V=424.8$ MeV fm^3, compared with our value of 425.5 MeV fm^3 given by Eq. (11). Another example is the Duke University potential,[14] selected to describe 7.0–26.0 MeV neutron data of singly- or doubly-closed-shell nuclei in the mass range $A=40$–208. At 10.0 this latter potential gives $J_V=417.4$ MeV fm^3, in excellent agreement with our value of 416.7 MeV fm^3.

The present J_V energy dependence [see Fig. 2(b)] may slightly deviate from linearity at the upper extreme of the present energy range. Such a trend was noted when we compared the predicted large-angle results shown in Figs. 1(a) and 1(b). A similar trend is suggested by the extrapolation to reported higher-energy data, as discussed below. However, these possible small J_V effects in the present ^{89}Y study are not of the character or the magnitude of those predicted in ^{40}Ca and ^{208}Pb by Mahaux and Ngô.[4] For several reasons it would be hard to unambiguously establish this nonlinearity as one goes to low energies. First, in the 3–4 MeV incident-neutron energy region, one has to estimate the compound-elastic-scattering cross section from a combination of known discrete states in ^{89}Y and from a statistical level formulation such as that of Gilbert and Cameron.[23] In this transitional energy region the level density, and hence the compound-elastic contribution, depends sensitively on the assumed nuclear temperature and that temperature may fluctuate rather sharply with energy. A misestimate of this quantity can lead to an anomalous energy dependence of J_V. These effects were a concern in the present study, primarily over the energy range 4.0–6.5 MeV and that is the range where the model description of the data shown in Figs. 1(a) and 1(b) is less good. Secondly, as one goes to lower energies fluctuations become important and a nonlinear variation of J_V, as suggested by the Fermi-surface anomaly, could be confused by experimentally fluctuating cross sections that preclude an average consistent with the basic concept of the optical model. Such fluctuations may have been a factor in the above interpretations at the low (2.75 MeV) energy.

Turning to the surface-derivative imaginary potential, we find that in order to fit the data over the entire energy range we need the energy-dependent geometry given in Eq. (4). Since the imaginary potential is introduced to account for channels involving neutron absorption, one would expect J_W to vary more dramatically from nucleus to nucleus than does J_V. This trend is supported by comparisons with Rapaport's global model[24] and by the prior interpretation of the ^{93}Nb neutron data.[7] On the other hand, the value of $J_W=61.7$ MeV fm^3 deduced for 7.75

MeV neutrons incident on ^{89}Y by the Stuttgart group[27] agrees very well with the 62.12 ± 2.49 MeV fm^3 obtained from our 7.5 MeV results. The energy dependencies of a_w and r_w can be qualitatively understood on the basis of the following arguments: The Pauli exclusion principle does not allow scattering into occupied states and hence, for low energies, only the tail of the nucleon distribution can contribute to neutron absorption, implying that $R_w=r_wA^{1/3}$ is large. However, as one goes to higher energies this blocking of states is less important, absorption moves further inside the nucleus, and the interaction will be less localized in r space.

The effect of the spin-orbit interaction is most evident in these interpretations near the 140° minima of the distributions, particularly at the higher energies. The above spin-orbit parameters were chosen so as to optimize the description of the data in the approximate angular range 120°–160°. The values given in Eq. (5) differ substantially from those reported by the Stuttgart group[27] from their interpretation of 7.75 MeV neutron elastic-scattering and polarization data. However, the present values are in reasonable agreement with those reported from other neutron-polarization studies in this mass region; for example, that of Ref. 14.

As a further check on the energy dependence of our conventional optical-model parameters [Eqs. (3)–(5) and (9)–(11)], we have looked at predictions beyond the present experimental energy range of 1.5–10.0 MeV. At low energies the s-wave strength function, derived from resonance experiments, is $S_0=(0.27\pm0.05)\times10^{-4}$.[28] This value is near the minimum of the S_0 distribution with mass, and may be subject to local energy fluctuations. Be that as it may, the prediction of our conventional model is a considerably smaller, $S_0=0.1\times10^{-4}$. This is really not surprising as not only are the above noted possible fluctuations a concern, but the calculated value of S_0 is extremely sensitive to the exact choice of r_w. A 5% reduction in the 1.5336 fm value given in Eq. (4) leads to nearly exact agreement between calculated and experimentally deduced values. Such a small change in r_w is well within the uncertainties associated with Eq. (4), and there is no assurance that the linear extrapolation of Eq. (4) will be very reliable at zero energy. Other aspects of the strength function are further noted below.

We have also extrapolated the conventional model to calculate the neutron total cross sections to 20 MeV, with the results shown in Fig. 6. These calculated results agree with the observed values, always to within 1.35%; i.e., to essentially the experimental uncertainty. This suggests that our conventional parametrization can be extrapolated over a wide energy range to represent the gross features of the n + ^{89}Y interaction, and supports the energy dependencies deduced from our analysis of the 1.5–10.0 MeV data. However, detailed descriptions of neutron differential-elastic scattering beyond the 1.5–10.0 MeV energy range may encounter some difficulty. Our linear extrapolations lead to only a mediocre description of the Ohio University 11.0 MeV elastic scattering data.[29] However, if we fix r_v, the imaginary-potential geometry and the spin-orbit potential to our general values and fit the Ohio data varying V, a_v, and W, we obtain a result as

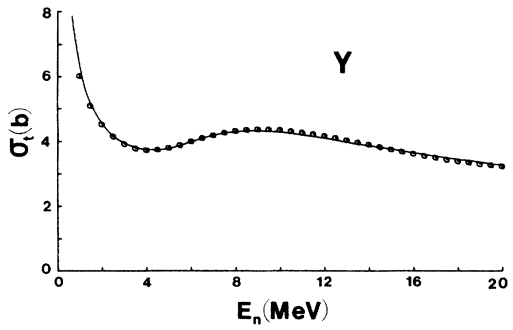

FIG. 6. Comparison of measured and calculated neutron total cross sections of ^{89}Y. The experimental values, as discussed in the text, are indicated by the curve taken from Ref. 10, and the calculated results are indicated by circular symbols.

good as reported in the original paper [judged on χ^2 of Eq. (2) and the author's reported uncertainties]. The resulting parameter values are $V=46.37$ MeV, $a_v=0.6764$ fm, and $W=9.28$ MeV, which give $J_V=424.9$ MeV fm^3 and $J_W=80.4$ MeV fm^3. These values are very similar to those obtained from a fit to our 10.0 MeV data: $J_V=427.8\pm7.9$ MeV fm^3 and $J_W=74.1\pm8.7$ MeV fm^3. This again suggests that the linear energy dependence of Eq. (11) is an oversimplification and that the slope of J_V decreases with increasing energy as suggested by the higher-energy values in Fig. 2(b). However, the effect, if present, is small; in fact, far short of that predicted in the ^{208}Pb region. Our 11.0 MeV parameters are qualitatively different than those of Ref. 29, demonstrating the nonunique nature of parameter sets and the merit of a systematic approach using an extensive data base.

In Sec. IV B we discussed an alternative fit to the data in which a surface-derivative real potential [Eqs. (14)] was added to the conventional Woods-Saxon term. The real radius, the imaginary-potential geometry, and the spin-orbit potential were fixed to the values of the conventional interpretation [Eqs. (3)–(5)], and V, a_v, and W were again varied to best fit the data. In contrast to the previous energy independence of a_v and J_W, for this surface-peaked real potential a_v and J_W take on a quadratic and linear energy dependence, respectively. The real Woods-Saxon depth, V, displays a slow decrease with energy. However, the rapid increase of a_v with energy leads to a volume integral, J_{WS}, for this potential that is energy independent. Thus the entire energy dependence of the total volume integral of the real potential [J_V of Eq. (18)] is governed by the energy dependence of the surface real interaction, Eqs. (14). We find that J_V decreases linearly with energy [see Fig. 5(b) and Eq. (19)], although the variation is not as strong as in the conventional optical-model analysis [see Eq. (11)].

In order to check the energy dependence of the real-surface-potential model, we again extrapolated our results well outside the 1.5–10.0 MeV energy range. The calculated S_0 strength function is 0.257×10^{-4}, in excellent agreement with the experimentally deduced value[28] of $(0.27\pm0.05)\times10^{-4}$. In order to use the model to calcu-

late the total cross section in the 10.0–20.0 MeV energy range, we need to know $J_W(E')$ for all E' in order to calculate ΔV [Eq. (14a)]. Our procedure for obtaining J_W was as follows.

(i) The imaginary potential to be used in the optical-model calculations was taken from Eqs. (4) and (17).

(ii) J_R, which determines $\lambda(E)$ of Eqs. (14), was calculated assuming

$$J_W = 0.673(E'+9.1)^2 \text{ MeV fm}^3 \text{ for } -18.2 \le E' \le 0 \text{ MeV},$$
$$J_W = 55.73 + 2E' \text{ MeV fm}^3 \text{ for } 0 \le E' \le 9.01 \text{ MeV},$$
$$J_W = 87.54 - 1.53E' \text{ MeV fm}^3 \text{ for } 9.01 \le E' \le 57.22 \text{ MeV}. \quad (20)$$

These assumptions are essentially equivalent to those discussed in Sec. IV B above, and when $J_W(E')$ is selected in this manner, it is continuous over the energy range $-18.2 \le E' \le 57.22$ MeV. With these ground rules, we find the extrapolation overestimates the total cross section at 11.0 MeV by 0.26% and underestimates it by 3.73% at 20.0 MeV. Certainly, the former is well within the experimental uncertainty, and the latter very possibly so. Thus we obtain nearly as good a prediction for the total cross section using the surface-peaked real potential as is obtained with the conventional potential, despite the large differences in the parametrizations.

In the analysis of the ^{93}Nb data,[7] we found that the entire energy dependence of J_V was due to the principal-value integral of Eq. (6). This result was also obtained in the present ^{89}Y analysis based upon a real potential consisting of the sum of Wood-Saxon and surface-derivative components. In Fig. 7 we plot

$$J_V = J_{WS} + J_R, \quad (21)$$

where J_{WS} has the energy-independent value given in Eq. (16), and J_R is the principal-value integral of Eq. (12) when $J_W(E')$ is parametrized by Eqs. (10). In the 2.0–10.0 MeV energy range the logarithmic energy dependence predicted in this way is barely distinguishable from the linear energy dependence given by either Eq. (11) or (19), as shown in Fig. 7. Below 2.0 MeV, Eq. (21) deviates from linearity and reaches a maximum at about −2.0 MeV. Because of our simplified assumption about $J_W(E')$ for $E' \le 0$ [see Eq. (10″)], one should probably not take seriously the predicted values of J_V below the Fermi energy, $E_F = -9.1$ MeV. However, it is interesting to note that in the range −9.0 to + 10.0 MeV, J_V given by Eq. (21) has much the same character as that predicted for ^{40}Ca and ^{208}Pb by Mahaux and Ngô.[4] The difference is that for the doubly-closed-shell nuclei the deviation from linearity is predicted to occur in the 6.0–7.0 MeV range, whereas for ^{89}Y the nonlinearity should only be evident below 2.0 MeV.

In Fig. 7 we have noted (by the symbol ○) the values of J_V together with their uncertainties, obtained in the conventional optical-model fit to our ^{89}Y data. × symbols denote the same results obtained using the real surface-derivative potential form (where uncertainties are omitted to avoid confusion). In all cases, except for the 5.9 MeV data, the ×'s lie within the error bars obtained in the conventional analysis. As noted above, the 5.9 MeV results are anomalous, but even in this case the error bars from the two different analyses overlap. Thus, either way of analyzing the ^{89}Y data leads to the result that the energy variation of J_V is consistent with a logarithmic dependence and this logarithmic dependence is essentially indistinguishable from a linear energy dependence over the region of the present measurements.

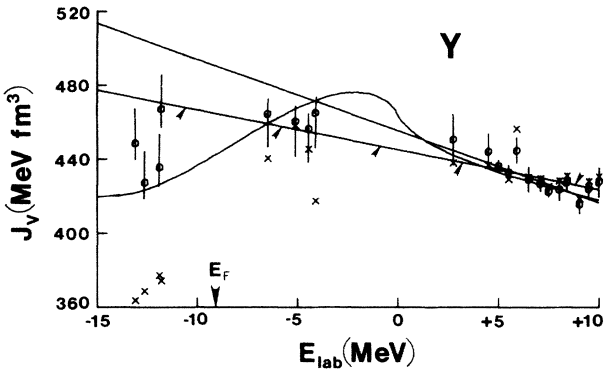

FIG. 7. A comparison of various predictions of J_V with experimental observations. The nonlinear curve shows the theoretical values of J_V given by Eq. (21) with $J_{WS} = 409.56$ MeV fm^3 and J_R calculated from Eqs. (10) and (12). The upper linear fit shows the result obtained using Eq. (11) and the lower one (curve with "tick" marks) the result with Eq. (19). The symbols ○ indicate the values deduced from the present experiments when a conventional optical model analysis was carried out. At negative energies, the same symbol denotes the values deduced when the particle- and hole-state binding energies are fitted using a real Woods-Saxon well. The symbols × indicate the corresponding results obtained when the surface-peaked real potential is included. The Fermi energy is indicated by E_F.

We also show in Fig. 7 the values of J_V needed to reproduce the binding energies of the single-particle and single-hole states in this mass region. Nuclear-structure studies near $A = 90$ indicate that, to a good approximation, ^{88}Sr can be considered a doubly magic nucleus.[30] Therefore, the available stripping and pickup data on ^{88}Sr were used, together with tables of nuclear masses,[31] to determine the experimental single-particle binding energies. For the $3s_{1/2}$ level in ^{89}Sr the data of Slater *et al.*[32] were taken, whereas for all other states the results of Blok *et al.*[33] were used. The requisite binding energies in MeV are −6.101 ($2d_{5/2}$), −4.77 ($3s_{1/2}$), −4.097 ($2d_{3/2}$), and −3.671 ($1g_{7/2}$) for the single-particle states relative to the ^{88}Sr core, and −12.665 ($1f_{5/2}$), −12.238 ($2p_{3/2}$), −11.502 ($2p_{1/2}$), and −11.333 ($1g_{9/2}$) for the hole states. Using the Thomas spin-orbit interaction of Eq. (5), the Woods-Saxon well depth was varied to reproduce these binding energies with r_v and a_v fixed to the values of Eqs. (3) and (9). The isospin dependence of Rapaport's global model[24] implies that the ^{89}Y potential should be 0.29 MeV deeper than found for ^{88}Sr. When this is taken into account, together with the fact that the potential expands as

$A^{1/3}$, the J_V results shown in Fig. 7 were obtained. The uncertainties that are assigned to the bound-state values reflect the fact that minor changes in the geometry of the well can change J_V by 2% without appreciably changing the binding energy. More important, any missing stripping strength would mean that the particle states are less tightly bound than we have assumed, leading to a smaller J_V value, whereas any missed pickup strength would mean that the hole states are more tightly bound, leading to larger values of J_V. It is for these reasons that the respective uncertainties shown in Fig. 7 are asymmetric. It is conservatively estimated that the missed strength could change the binding energy by 1.0 MeV. The values of J_V needed to fit the four single-particle energies are clustered around 461.6 MeV fm^3 with a rms deviation of 3.5 MeV fm^3. Their values are fitted equally well by either Eq. (19) or Eq. (21), and are also consistent with a flattening out of the J_V versus energy curve in the -4.0 to -6.0 MeV energy region.

For the $1g_{9/2}$ hole state the value of J_V is 467.0 MeV fm^3 and, considering the uncertainties in stripping and pickup data and possible variations in well parameters, we conclude that this hole-state value is essentially the same as that obtained for the above particle states. The remaining hole-state J_V values, particularly those for the $2p$ states, are substantially smaller. However, these results depend sensitively on the assumed spin-orbit interactions. For example, in our ^{93}Nb analysis[7] we assumed a Woods-Saxon well with $a_v=0.698$ fm and $r_v=1.25$ fm, and that the spin-orbit potential had a strength of 6.0 MeV with the same geometry. In that case, the J_V's for the $1f_{5/2}$, $2p_{3/2}$, and $2p_{1/2}$ hole states were all approximately 11% smaller than for the $1g_{9/2}$ level. With the present spin-orbit interaction, Eq. (5), the $1f_{5/2}$ value is less than 4% smaller than that for the $l=4$ state, and on the average the $2p$ values are $7\frac{1}{2}$% smaller. Although some change in the spin-orbit interaction may bring the J_V of these four hole states closer together, one must conclude, at present, that either substantial $2p$ and $1f$ pickup strength has been missed and/or that the J_V integrals show a marked variation over a small binding-energy range.

For completeness, we also indicate with $\times$'s in Fig. 7 the J_V values that are needed to give the correct binding energies when the real potential includes the surface-derivative component. The derivative real potential was assumed to have the a_w and r_w values given in Eq. (4) with $E=0$ and a strength equal to that required to give the value of $J_R(E)$ computed from Eqs. (10) and (12). The spin-orbit interaction was assumed to be that of Eq. (5) and the Woods-Saxon well depth, V_0, was varied so as to reproduce the experimental results when $r_v=1.24$ fm and $a_v=0.1916$ fm, the value of a_v deduced with this model when $E=0$ [see Eqs. (15)]. Because a_v is small, the Woods-Saxon well has a fairly sharp surface (i.e., approaches a square well). It is known[34] that such a well tends to bind high l states more tightly and hence, to achieve a given binding energy, one requires a smaller V_0 and J_V. Furthermore, the tightly bound hole states have wave functions that do not extend very far into the diffuse surface of the well and thus, for all intents and purposes, these states experience a square well potential. Consequently, in all cases, and particularly for hole states, the required V_0 values are smaller than for the conventional fit where $a_v=0.7$ fm. The larger the l value the larger the decrease in J_V.

In summary, we have fitted neutron total and differential-elastic-scattering cross sections of ^{89}Y over the energy range 1.5–10.0 MeV using the optical-statistical model. The fitting was carried out using two variants of this model. First, a conventional analysis was made in which the real potential had the Woods-Saxon form, the imaginary a derivative Woods-Saxon shape, and the spin-orbit potential was the Thomas term. In the second analysis, the foregoing potentials were used with the addition of a real surface-derivative Woods-Saxon potential, as required by dispersion relationships.[3] Independent of the model used in the analysis, we conclude the following.

(i) In order to fit the data over the present energy range, the geometry of the imaginary potential must be energy dependent, with the radius decreasing and the diffuseness increasing with incident energy.

(ii) The energy dependence of J_V, the volume integral of the real potential, is consistent with the predictions of Eq. (21). In this equation J_{WS} is constant and the entire energy dependence of J_V comes from J_R; that is, from the principal value integral of Eq. (6).

(iii) Although J_R is actually a logarithmic function of energy, in the present energy range it is almost identical to a linearly decreasing function of energy. Thus the neutron total and differential-elastic-scattering cross sections of ^{89}Y show no evidence for the Fermi-surface anomaly, over the present 1.5–10.0 MeV energy range, of the character and magnitude reported in the $A=40$ and 208 regions. This conclusion is consistent with results previously obtained for ^{93}Nb.[7]

ACKNOWLEDGMENTS

The authors are indebted to a number of members of the Applied Physics Division, Argonne National Laboratory, for their assistance and consultation in the above work. This work was supported by the U.S. Department of Energy.

[1]G. E. Brown, J. H. Gunn, and P. Gould, Nucl. Phys. **46**, 598 (1963).

[2]J. Blomqvist and S. Wahlborn, Ark. Fys. **16**, 545 (1960).

[3]See, for example, G. R. Satchler, *Direct Nuclear Reactions* (Clarendon, Oxford, 1983).

[4]C. Mahaux and H. Ngô, Nucl. Phys. **A378**, 205 (1982); Phys. Lett. **100B**, 285 (1981).

[5]R. W. Finlay, J. R. M. Annand, J. S. Petler, and F. S. Dietrich, Phys. Lett. **155B**, 313 (1985).

[6]J. R. M. Annand, R. W. Finlay, and F. S. Dietrich, Nucl. Phys. **A443**, 249 (1985).

[7]A. B. Smith, P. T. Guenther, and R. D. Lawson, Argonne Na-

tional Laboratory Report No. ANL/NDM-91, 1985 (unpublished); Nucl. Phys. **A455**, 344 (1986).

[8]A. Smith, P. Guenther, R. Larsen, C. Nelson, P. Walker, and J. Whalen, Nucl. Instrum. Methods **50**, 277 (1967).

[9]C. Budtz-Jørgensen, P. Guenther, J. Whalen, W. McMurray, M. Renan, I. van Heerden, and A. Smith, Z. Phys. A **319**, 47 (1984).

[10]A. Smith, D. Smith, P. Rousset, R. D. Lawson, and R. Howerton, Argonne National Laboratory Report No. ANL/NDM-94, 1986 (unpublished).

[11]*IAEA Technical Report No. 227,* edited by H. Condé, A. Smith, and A. Lorenz (IAEA, Vienna, 1983), p. 3; see also the evaluated data file ENDF/B-V available from the National Nuclear Data Center, Brookhaven National Laboratory.

[12]P. T. Guenther, Ph.D. thesis, University of Illinois, 1977.

[13]W. Kinney and F. Perey, Oak Ridge National Laboratory Report No. ORNL-4552, 1970 (unpublished).

[14]R. L. Walter and P. P. Guss, in *Nuclear Data for Basic and Applied Science,* edited by P. G. Young, R. E. Brown, G. F. Auchampaugh, P. W. Lisowski, and L. Stewart (Gordon and Breach, New York, 1986), Vol. 2, p. 1079; R. Walter and J. Delaroche, in Specialist's Meeting on Use of the Optical Model for the Calculation of Neutron Cross Sections Below 20 MeV, Report No. NEANDC-222U, OECD Nuclear Energy Agency, Paris, 1986, p. 271 (unpublished).

[15]P. E. Hodgson, *Nuclear Reactions and Nuclear Structure* (Clarendon, Oxford, 1971).

[16]A. Smith, P. Guenther, and J. Whalen, Nucl. Phys. **A415**, 1 (1984).

[17]A. Smith, P. Guenther, and J. Whalen, Argonne National Laboratory Report No. ANL/NDM-70, 1982 (unpublished).

[18]See A. M. Lane and A. Thomas, Rev. Mod. Phys. **30**, 257 (1958).

[19]P. A. Moldauer, private communication.

[20]W. Hauser and H. Feshbach, Phys. Rev. **87**, 366 (1952).

[21]P. A. Moldauer, Nucl. Phys. **A344**, 185 (1980).

[22]C. Lederer and V. Shirley, *Table of Isotopes,* 7th ed. (Wiley, New York, 1978).

[23]A. Gilbert and A. Cameron, Can. J. Phys. **43**, 1446 (1965).

[24]J. Rapaport, Phys. Rep. **87**, 25 (1982).

[25]R. Sartor and C. Mahaux, Phys. Rev. C **21**, 1546 (1980).

[26]I. Ahmad and W. Haider, J. Phys. G **2**, L157 (1976).

[27]G. Schreder, W. Grum, K.-W. Hoffman, G. Schleussner, and J. W. Hammer, University of Stuttgart, Report No. NEANDC(E)-262U, 1985 (unpublished).

[28]S. Mughabghab, M. Divadeenam, and N. E. Holden, in *Neutron Cross Sections* (Academic, New York, 1981), Vol. 1, Pt. A.

[29]Yan Yiming C. E. Brient, R. W. Finlay, G. Randers-Pehrson, A. Marcinkowski, R. C. Tailor, and J. Rapaport, Nucl. Phys. **A390**, 449 (1982).

[30]F. J. D. Serduke, R. D. Lawson, and D. H. Gloeckner, Nucl. Phys. **A256**, 45 (1976).

[31]A. H. Wapstra and K. Bos, At. Data Nucl. Data Tables **19**, 177 (1977).

[32]D. C. Slater, E. R. Cosman, and D. J. Pullen, Nucl. Phys. **A206**, 433 (1973).

[33]H. Blok, W. R. Zimmerman, J. J. Kraushaar, and P. A. Batay-Csorba, Nucl. Phys. **A287**, 156 (1977).

[34]A. A. Ross, Hans Mark, and R. D. Lawson, Phys. Rev. **102**, 1613 (1956).